The Journal of Green Energy and Environmental Engineering

Research Paper

Effect of MnO_2 Modification on Structure and Dielectric Properties of $K_{0.5}Na_{0.5}NbO_3$ Ceramics

Lucas Eklund[1], Romualdo Hatfield[1], Daiany Filho[2], Tiago Shrestha[2,*]

[1] School of Engineering Science, Lappeenranta University of Technology, P.O. Box 20, FI-53850, Lappeenranta, Finland
[2] Departamento de Zootecnia, Universidade Federal de Viçosa, Viçosa 36571-000, Minas Gerais, Brazil
*Corresponding author: tiagoshrestha.AS23@ufv.br

Abstract. This study investigates the effect of manganese dioxide (MnO_2) doping on the structural and dielectric properties of potassium sodium niobate ($K_{0.5}Na_{0.5}NbO_3$, KNN) ceramics. KNN ceramics with varying MnO_2 concentrations were synthesized via the solid-state reaction method, and their dielectric properties were comprehensively characterized. The results indicate that all MnO_2-doped KNN ceramic samples exhibit a typical tetragonal perovskite structure. An appropriate amount of MnO_2 doping significantly enhances the dielectric properties of KNN ceramics. However, excessive doping leads to performance degradation, although the properties remain superior to those of pure KNN ceramics. Under optimal MnO_2 doping conditions, the dielectric constant gradually increases, indicating enhanced polarization intensity and dielectric performance. Furthermore, MnO_2 doping reduces the dielectric loss of KNN ceramics. At low frequencies, the dielectric constant of all KNN ceramic samples increases with temperature due to structural changes induced by doping; however, beyond a specific temperature threshold, the dielectric constant begins to decline. This finding is crucial for electronic devices operating within particular temperature ranges.

Keywords: *Potassium sodium niobate; Doping; Dielectric constant; Impedance; Voltage withstand strength*

Received on 26 Jan 2026, Accepted on 15 April 2026, Published on 15 May 2026

1 Introduction

The global transition toward sustainable industrialization and green electronics has intensified the demand for environmentally benign functional ceramics that can replace legacy lead-based materials without compromising performance. For decades, lead zirconate titanate (PZT)-based ceramics have dominated the market for actuators, sensors, transducers, and multilayer ceramic capacitors (MLCCs), owing to their exceptional piezoelectric coefficients (d_{33} > 300 pC/N), high Curie temperatures (TC), and robust dielectric properties [1, 2]. However, the toxicity of lead oxide (PbO), which constitutes over 60% by weight in PZT, poses severe environmental and health risks. PbO is volatile during high-temperature sintering, leading to toxic emissions, and the potential leaching of lead from discarded devices threatens ecosystems and human health. In response, stringent international regulations—such as the European Union's Restriction of Hazardous Substances (RoHS) directive, the Waste Electrical and Electronic Equipment (WEEE) directive, and China's National Sword Policy—have mandated the elimination of lead from electronic materials, transforming the development of high-performance lead-free alternatives from a scientific curiosity into an industrial imperative [3, 4].

Among the numerous lead-free candidates explored, potassium sodium niobate ($K_{0.5}Na_{0.5}NbO_3$, KNN)-based ceramics have emerged as one of the most promising substitutes. KNN possesses a perovskite structure with a high TC(~420°C), ensuring thermal stability in high-temperature applications such as automotive sensors and aerospace actuators [5, 6]. Its constituent elements—potassium, sodium, and niobium—are abundant, low-cost, and environmentally benign, aligning with circular economy principles. Additionally, KNN exhibits a favorable combination of spontaneous polarization (Ps) and coercive field (Ec), making it suitable for both piezoelectric and dielectric applications. Despite these advantages, the practical implementation of KNN is hindered by three intrinsic limitations. First, the volatility of alkali metal oxides (K_2O and Na_2O) during sintering induces stoichiometric deviations, pore formation, and microcracking, severely degrading electrical properties [7].

Second, the polymorphic phase boundary (PPB) in KNN—critical for enhancing piezoelectric performance—is highly sensitive to composition and temperature fluctuations, making reproducible manufacturing challenging [7]. Third, the dielectric properties of pure KNN, particularly its dielectric constant (εr~ 300–400) and loss tangent (tan δ ~ 2–3%), fall short of the requirements for high-capacitance MLCCs, which demand εr> 2000 and tan δ < 1% [8].

To overcome these bottlenecks, researchers have pursued two primary modification strategies: chemical doping and process optimization. Chemical doping involves the introduction of aliovalent ions (e.g., Li^+, Ta^{5+}, Sb^{5+}) to stabilize the desired phase structure and improve electrical properties. For instance, Li/Ta co-doping shifts the PPB to room temperature, significantly boosting d_{33} [9]. However, these modifications often rely on expensive raw materials (e.g., Ta_2O_5, Sb_2O_3) and complex synthesis routes, increasing production costs. Process optimization techniques—such as hot pressing (HP) and spark plasma sintering (SPS)—can produce dense KNN ceramics with fine grains, but these methods are energy-intensive, require specialized equipment, and are unsuitable for large-scale production of complex-shaped components [11].

Recently, transition metal oxide doping—particularly with manganese dioxide (MnO_2)—has gained traction as a cost-effective and versatile approach to refine the microstructure and electrical properties of KNN. Manganese ions exhibit variable valences (Mn^{2+}, Mn^{3+}, Mn^{4+}) and can occupy both A-sites (K/Na sites) and B-sites (Nb sites) in the perovskite lattice or segregate at grain boundaries, enabling multi-scale control of defect chemistry and domain dynamics [12, 13]. Existing studies report that MnO_2 can promote liquid-phase sintering by forming low-melting eutectics with alkali oxides, facilitating grain growth and densification, which reduces porosity-related dielectric loss [14]. Additionally, Mn doping is known to modify the concentration of oxygen vacancies ($V_O^{\bullet\bullet}$), which are pivotal for domain wall motion and electrical conductivity. For example, Deng et al. [14] demonstrated that MnO_2 doping in KNN creates defect dipoles that pin domain walls, enhancing piezoelectric strain. However, the literature presents a complex and sometimes contradictory picture: while some studies highlight MnO_2's ability to improve piezoelectric properties, others report that excessive doping leads to abnormal grain growth, secondary phase formation, and compromised mechanical strength [10, 15].

Crucially, the specific impact of MnO_2 doping on the dielectric relaxation, temperature stability, and non-Ohmic conduction behavior of KNN remains insufficiently characterized. Most prior work focuses on piezoelectric performance, with limited systematic investigation of how MnO_2 concentration governs the evolution of dielectric properties across broad frequency (40 Hz–10^6 Hz) and temperature (RT–300°C) ranges. Furthermore, the underlying defect chemistry mechanisms—such as the role of Mn-induced oxygen vacancies and their interaction with domain walls—are not fully elucidated. For instance, Jiang et al. [15] observed that MnO_2 doping in 0.97KNN-0.03BKT ceramics reduces dielectric loss but increases the Curie temperature, while Lopez-Juarez et al. [22] reported that Mn doping enhances dielectric constant at low frequencies but degrades high-frequency performance. These inconsistencies underscore the need for a comprehensive, concentration-dependent study to clarify the structure-property relationships in MnO_2-doped KNN.

Addressing these gaps, this study systematically investigates the effect of MnO_2 doping (0–0.095 mol%) on the structural evolution and dielectric properties of $K_{0.5}Na_{0.5}NbO_3$ ceramics prepared via the conventional solid-state reaction method. The specific objectives are threefold: (1) Microstructural Engineering: To elucidate how MnO_2 concentration influences sintering kinetics, phase purity, and grain morphology, with a focus on the transition from solid-state to liquid-phase sintering. (2) Dielectric Performance Optimization: To evaluate the frequency (40 Hz–10^6 Hz) and temperature (RT–300°C) dependent dielectric response, identifying the optimal doping level that maximizes dielectric constant while minimizing loss. (3) Mechanism Elucidation: To establish a comprehensive structure-property relationship by analyzing impedance spectroscopy, conductivity behavior, and non-Ohmic J-Echaracteristics, thereby clarifying the role of Mn-induced defect dipoles and oxygen vacancies in governing electrical behavior. By bridging fundamental defect chemistry with practical dielectric performance, this work provides a pathway for designing high-performance, lead-free KNN ceramics tailored to specific electronic applications.

2. Experimental

2.1 Raw Materials

The primary raw materials for preparing MnO_2-doped $K_{0.5}Na_{0.5}NbO_3$ (KNN-x%Mn) ceramics and their mass fractions were: Na_2CO_3 (99.8%), K_2CO_3 (99.0%), Nb_2O_5 (99.99%), and MnO_2 (99.9%). Here, xrepresents the molar percentage of MnO_2 incorporated into $K_{0.5}Na_{0.5}NbO_3$, with values of 0.010%, 0.020%, 0.035%, 0.060%, and 0.095%.

2.2 Sample Preparation

First, raw materials were weighed according to stoichiometric ratios and placed into a nylon ball milling jar with ethanol (99.7%) and planetary ball milled for 24 h with activators. Second, the dried mixture was calcined in a furnace at 800–900 °C for 2 h, followed by regrinding. Finally, polyvinyl alcohol (PVA) was added as a binder, and the mixture was pressed into cylindrical samples with a diameter of 10 mm. The obtained samples were sintered in a tube furnace at 1050–1070 °C for 3 h. Subsequently, to measure electrical properties, polarization treatment was performed at an electric field strength of 2 kV/mm for 20 min. Simultaneously, spherical samples were coated with silver paste and sintered at 750 °C for 10 min.

2.3 Sample Characterization

The phase structure of the ceramics was characterized by X-ray diffraction (XRD, Rigaku ULTIMAIV) using Cu Kα radiation, with a scanning speed of 2 °/min and a step size of 0.02°. The cross-section of the ceramics was observed using scanning electron microscopy (SEM, Zeiss Sigma 300). Dielectric properties were measured using an LCR meter (TH2829, 20 Hz–1 MHz) over a frequency range of 40 Hz to 10^6 Hz. The dielectric constant was subsequently determined by considering the measured thickness and capacitance.

3. Results and Discussion

3.1 Microstructure and Morphology

Figure 1 shows scanning electron microscopy (SEM) images of the fracture surfaces of pure KNN ceramics and KNN ceramics doped with different concentrations of MnO_2. It is evident from Figure 1 that the incorporation of MnO_2 significantly influences the grain size of KNN ceramics. The average grain size of pure KNN is approximately 1.2 μm, whereas that of KNN doped with 0.01% MnO_2 is about 1.8 μm. In contrast, the average crystal sizes of samples doped with 0.020%, 0.035%, 0.060%, and 0.095% MnO_2 are close to 3.5 μm. Under optimal sintering conditions, Orayech et al. [16] reported KNN crystal sizes exceeding 3 μm. Changes in grain size are primarily influenced by liquid-phase sintering, with corresponding evidence found in Li^+ and Cu^{2+} doped KNN ceramics [17–18]. When Mn is incorporated into KNN ceramics, manganese oxides form eutectics with other components in the KNN matrix (e.g., Na_2O, K_2O) at temperatures lower than the melting point of pure KNN. This implies that a small amount of liquid second phase appears between particles during sintering, achieving liquid-phase sintering. At this point, the sintering mechanism shifts from slow solid-state diffusion to an efficient liquid-phase-assisted "dissolution-precipitation" mechanism. This process strongly stimulates the transport of matter from small grains to precipitate in coarse-grained, low-surface-energy regions, macroscopically manifesting as a significant increase in average grain size, consistent with the grain size variation observed in Figure 1.

Figure 2 presents the energy-dispersive spectroscopy (EDS) analysis of the KNN-0.060%Mn ceramic sample. It is visible from Figure 2 that elements such as O, Na, K, Mn, and Nb exist at different locations. Most manganese elements are uniformly distributed, while a small portion is concentrated, primarily adhering to the ceramic grain boundaries. As shown in the EDS spectrum in Figure 2(b), all elements in the sample were detected, and peaks for Mn were observed at 0.26 keV and 5.86 keV, indicating the presence of manganese oxide (MnO_2).

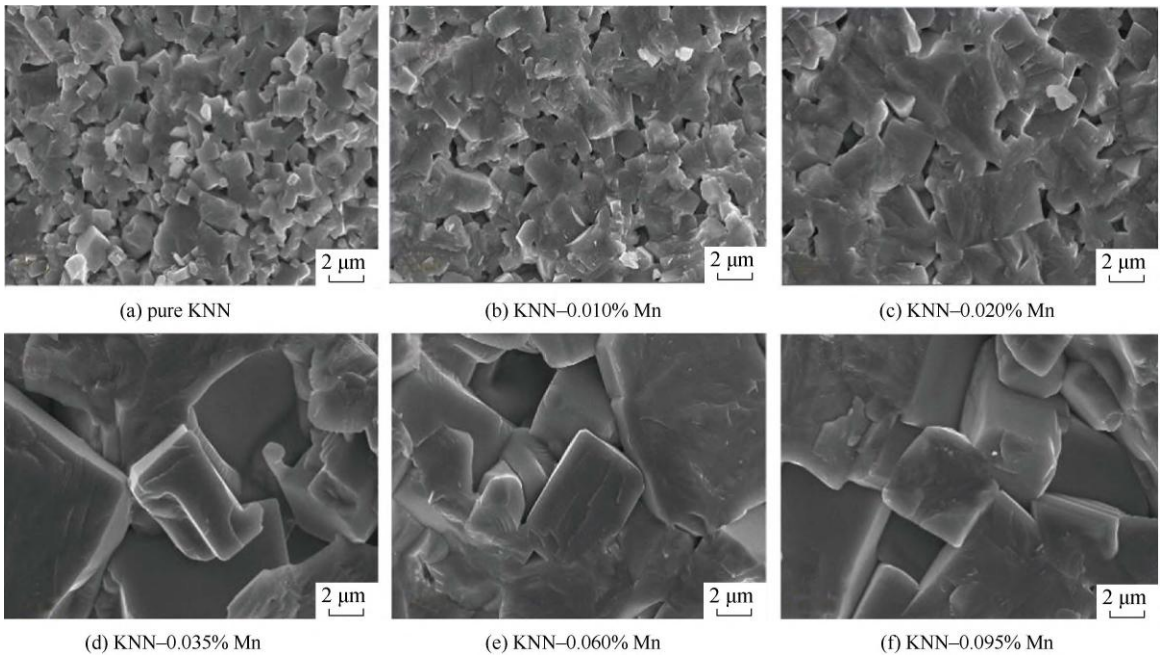

Figure 1 SEM images of fracture surfaces of the KNN and KNN ceramics doped with different amounts of MnO_2.

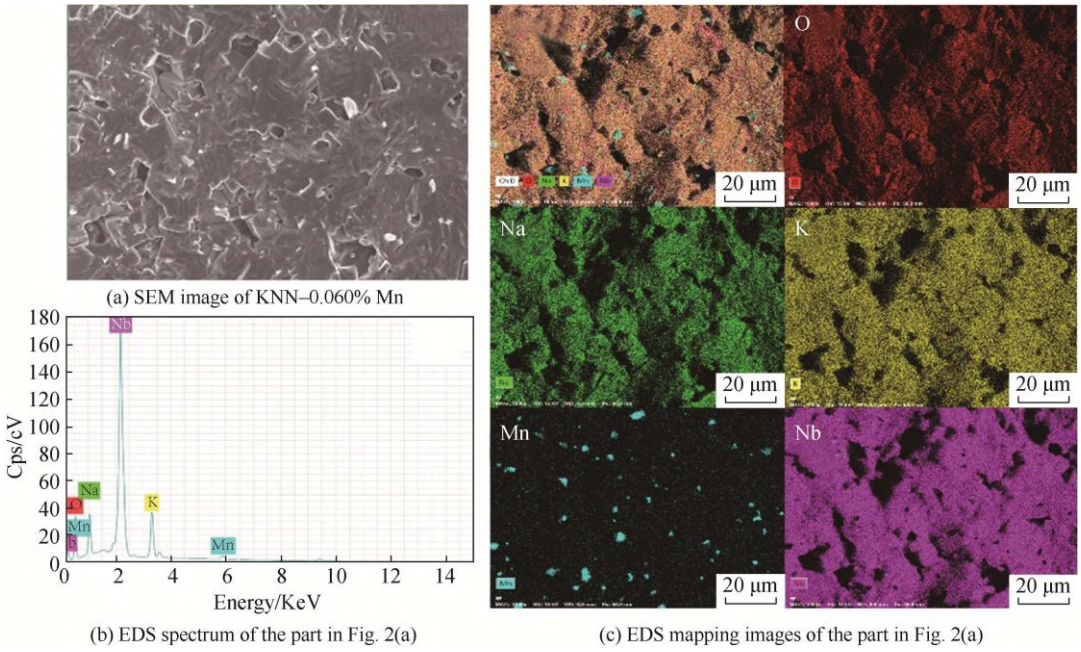

Figure 2 EDS analysis of KNN-0.060% Mn.

3.2 Phase Analysis

Figure 3 shows the XRD patterns of KNN-x%Mn ceramics sintered in air. It is visible from Figure 3 that no obvious impurity phases were observed in all MnO_2-doped KNN ceramic samples [19], suggesting that manganese ions have been incorporated into the perovskite lattice. In pure KNN ceramic samples, tetragonal (O), rhombohedral (R), and tetragonal prismatic (T) phases were observed.

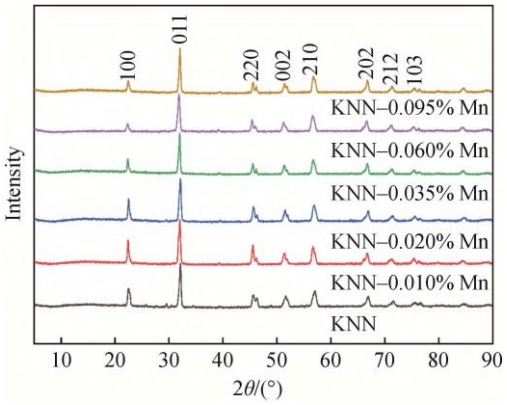

Figure 3 XRD patterns of KNN-x%Mn ceramics sintered in the air.

The diffraction peaks at 22° and 46° exhibit characteristics of low front intensity and high rear intensity, indicating that all MnO_2-doped KNN ceramic samples possess a typical tetragonal perovskite structure, which is fundamental to their density and piezoelectric properties [20]. The splitting of the (220)/(002) peak around 2θ = 46° indicates the presence of a single tetragonal phase. Simultaneously, the intensity ratio I(200)/I(002) varies with doping levels, suggesting the presence of a rhombohedral phase. Furthermore, after adding Mn elements, although no second-phase diffraction peaks related to Mn appeared, the (220)/(002) peak position of MnO_2-doped KNN ceramics shifted significantly toward lower angles compared to pure KNN. This phenomenon is attributed to the presence of manganese ions with different valences (Mn^{2+}, Mn^{3+}, and Mn^{4+}) in the doped ceramics. The vast majority of Mn does not form new phases with distinctly different stoichiometries but dissolves into the KNN lattice during the late sintering stage, forming solid solutions; therefore, no new diffraction peaks are generated, but it causes minor changes in the lattice constants of the KNN main phase. The remaining trace Mn exists at grain boundaries in oxide form; since these second phases are present in extremely low quantities, they were not detected by XRD characterization, but Mn aggregation was observed in specific regions via EDS mapping in Figure 2.

3.3 Dielectric Property Analysis

Figure 4 shows the frequency-dependent variation curves of dielectric permittivity and dielectric loss factor for KNN ceramics doped with different concentrations of MnO_2 at room temperature. It is evident from Figure 4 that the incorporation of MnO_2 significantly increases the dielectric constant of KNN ceramics. In the low-frequency band, the sample's dielectric constant increases proportionally with the MnO_2 incorporation amount, indicating improved polarization intensity and overall dielectric performance. However, within the frequency range of 10^2–10^6 Hz, the dielectric constant initially increases with increasing manganese oxide concentration but subsequently decreases gradually. The maximum value occurs at a doping level of 0.060%, indicating that this is the optimal doping level. Within the low doping range (0–0.060%), Mn incorporation promotes liquid-phase sintering, reduces porosity, and greatly improves the densification of the ceramic body. Simultaneously, Mn incorporation into the KNN ceramic interior leads to grain growth and a reduced grain boundary ratio, contributing to higher overall dielectric constant levels. When the doping level exceeds 0.060%, Mn ions exist mainly as Mn^{2+} and Mn^{3+} in KNN, substituting for Nb^{5+} at the B-site. Due to the different valences, acceptor doping becomes dominant, forming "acceptor-oxygen vacancy" pairs that tightly pin domain walls, hindering domain wall flipping and movement under alternating electric fields. Dielectric constant (especially in ferroelectric materials) derives significantly from domain wall contributions, and "domain pinning" severely impairs polarization response, leading to a significant decrease in dielectric constant. In addition to the effects of oxygen vacancy defects, excess Mn cannot be fully dissolved into the KNN lattice and precipitates at grain boundaries as Mn-rich second phases. If these second phases possess low dielectric constants or increase grain boundary resistance, they cause an overall decline in dielectric constant. Even if their content is too low to be detected by XRD, their negative impact on polarization and dielectric constant may still exist.

Furthermore, all measured dielectric constant curves show a downward trend with increasing frequency at room temperature. This behavior can be attributed to the dominant role of space charge polarization and polarizing

molecules at lower frequencies [21]. Between 10^2 Hz and 10^6 Hz, the curves exhibit an almost horizontal downward trend, resulting from the high resistance inside the ceramic material hindering polarization reversal speed. Alternatively, at higher frequencies, polarization becomes decoupled from frequency, leading to a decrease and stabilization of dielectric constant values [22]. Due to different response times of microscopic polarization mechanisms, the macroscopic dielectric constant inevitably functions as a frequency variable. Resistance is a key factor controlling the response time of slow polarization mechanisms. Resistance reflects the hindrance to carrier movement within the material. High resistance indicates that internal charges move with difficulty. At low frequencies (e.g., 10^2 Hz), the electric field changes slowly, providing ample time for charges to complete the reversal process. Consequently, almost all types of polarization can keep pace with field changes and contribute to the dielectric constant; thus, the highest dielectric constant is measured at this stage. At high frequencies, polarization mechanisms with slow frequency responses, such as space charge polarization, cannot follow the field changes due to their inherently slow polarization speed combined with high resistance hindrance. These polarization behaviors begin to respond just as the field direction reverses. Therefore, they fail to contribute to the final polarization intensity. Once the dielectric constant drops to a lower level, it basically no longer changes with frequency, and the curve becomes flat and stable.

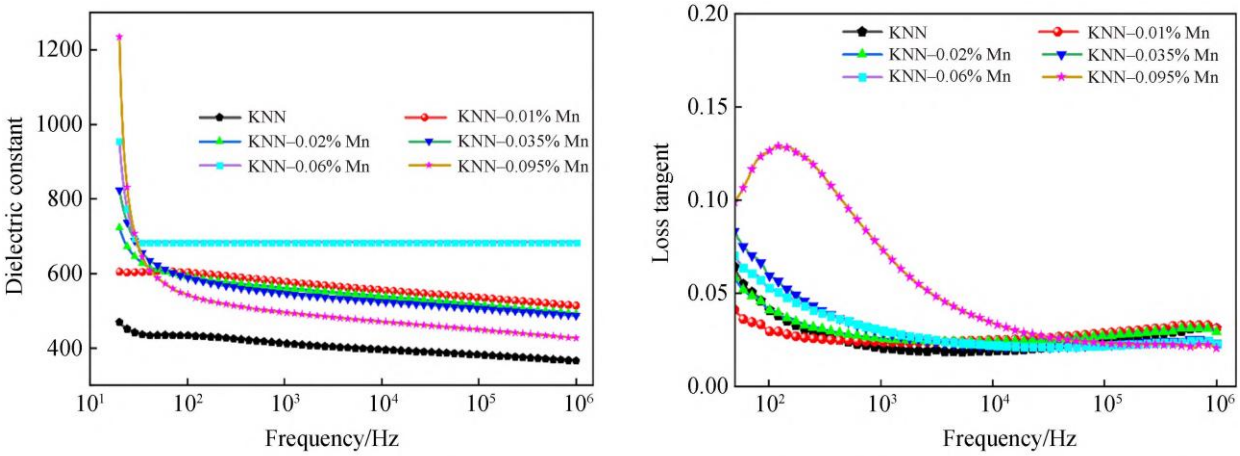

(a) Dielectric permittivity for MnO_2-doped KNN ceramics with varying concentrations

(b) Dielectric loss factor for MnO_2-doped KNN ceramics with varying concentrations

Figure 4 Frequency-dependent variations of dielectric permittivity and dielectric loss factor at room temperature for MnO_2-doped KNN ceramics with varying concentrations.

Dielectric loss curves measured at room temperature decrease with increasing frequency. This can be attributed to the acceleration of electron movement within grains surpassing the polarization speed of grain boundaries and defects, thereby reducing charge movement and leakage, leading to decreased dielectric loss. Alternatively, this phenomenon can be explained by the Debye relation [23]. According to Debye, in the low-frequency region, the value of tan δ is inversely proportional to frequency. This ceramic material exhibits dielectric dispersion in the low-frequency range, which is common in ferroelectric materials; conversely, no dielectric dispersion was observed in the high-frequency region, suggesting that interfacial space charges dominate at lower frequencies causing this dispersion phenomenon [24]. At low frequencies, the sample's dielectric loss factor decreases with increasing MnO_2 doping amount, indicating that manganese oxide doping promotes grain size uniformity and reduces intergranular gaps, thereby increasing ceramic density. Increased density reduces leakage current between particles, thereby lowering the dielectric loss factor. In the medium and high-frequency ranges, there is no significant difference in dielectric loss among all samples, as their curves highly overlap. However, within the frequency range of 10^2 Hz to 10^6 Hz, the dielectric loss curve value of the sample doped with 0.095% MnO_2 is higher than that of other samples. Several factors need consideration for this scenario: 1) Polarization phenomena at grain boundaries and internal defects become more pronounced in this frequency range, leading to charge movement and leakage, increasing dielectric loss; 2) This frequency range enhances the skin effect, shortening the path of current in conductors and reducing the effective width of the equivalent cross-section. Consequently, equivalent resistance increases, and accompanying losses rise; 3) Within this frequency range, the natural vibration frequency of the sample temporarily approaches its self-resonant frequency, causing increased

dielectric loss; 4) Parasitic capacitance and inductance exist transiently in the circuit within this frequency range, leading to increased oscillation current. These factors, combined with increased resistance due to heat loss during current conduction, further amplify losses; 5) Pore formation increases defect density within samples, leading to an overall rise in dielectric loss [25].

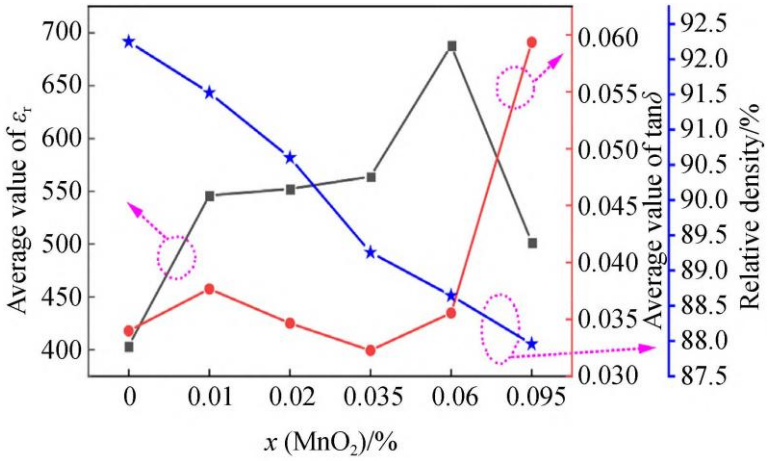

Figure 5 Relationship between the relative density and the dielectric properties of KNN-x%Mn ceramic samples.

Figure 5 shows the relationship curves between the relative density of KNN-x%Mn ceramic samples and their dielectric properties. It can be seen from Figure 5 that as MnO_2 doping increases from 0 to 0.060%, the average dielectric constant increases correspondingly, while average dielectric loss slightly increases but not significantly. However, when MnO_2 doping increases to 0.095%, average dielectric constant begins to drop rapidly, and average dielectric loss also increases rapidly. This aligns with the phenomenon that relative density decreases with increasing MnO_2 doping, as the ionic radius of manganese differs from existing potassium, sodium, and niobium ions in KNN ceramics, causing lattice distortion. Simultaneously, manganese doping leads to the formation of new phases in KNN ceramics, so when doping levels are higher, more manganate phases or other heterogeneous phases form, changing the ceramic microstructure and increasing more interfacial voids or discontinuities, thereby reducing overall relative density.

3.4 Temperature Dependence of Dielectric Properties

Since the temperature characteristics of ceramic capacitors are also a metric for evaluating performance, internal microscopic physical movements of ceramics are susceptible to temperature influence. To highlight the adaptability of this work's results in different temperature environments and expand application scenarios, temperature spectrum analyses were performed on dielectric and conductivity properties. Results indicate that the dielectric constant of all KNN-x%Mn ceramic samples increases with rising temperature, but after reaching a certain temperature (240 °C for KNN ceramics, 200 °C for MnO_2-doped KNN ceramics), it decreases as temperature drops. Therefore, KNN ceramic samples and samples with 0.060% MnO_2 doping were selected as representatives, and their dielectric constant and dielectric loss were studied.

Figure 6 shows the relationship curves of dielectric constant and dielectric loss factor with temperature variation for KNN ceramics and KNN ceramics doped with 0.060% MnO_2. Figures 6a–d show that regardless of temperature, their dielectric constant and dielectric loss exhibit a decreasing trend with increasing frequency. To better determine the optimal operating frequency and temperature of the samples, the relationship between dielectric constant and dielectric loss with temperature was studied at frequencies of 20, 10^2, 10^3, 10^4, 10^5, and 10^6 Hz. At 20 Hz, although the dielectric constant increases rapidly with temperature, its stability is extremely poor. Upon reaching a certain temperature, the dielectric constant declines continuously, attributed to increased molecular thermal vibration and dipole disorder [26]. At frequencies of 10^2, 10^3, 10^4, 10^5, and 10^6 Hz, although dielectric constant increases slowly with temperature, its stability is excellent. Furthermore, whether at low, medium, or high frequencies, 240 °C and 200 °C are the temperatures where dielectric constant reaches optimum for KNN

ceramics and MnO_2-doped KNN ceramics, respectively. Figures 6f and 6h show that at 20 Hz frequency, dielectric loss increases rapidly with temperature. The sharp upward trend in dielectric loss at higher temperatures results from lattice defect generation caused by high sintering temperatures [26]. At 10^1 Hz and 10^2 Hz frequencies, dielectric loss becomes extremely unstable with rising temperature. At 10^3, 10^4, 10^5, and 10^6 Hz frequencies, dielectric loss changes stably with temperature. Moreover, whether at low, medium, or high frequencies, 240 °C and 200 °C are the temperatures where dielectric loss is lowest for KNN ceramics and MnO_2-doped KNN ceramics, respectively. Therefore, comprehensive analysis of Figure 6 reveals that under temperature conditions of 200 °C to 240 °C and frequency conditions of 10^4 Hz to 10^6 Hz, the dielectric performance of KNN-x%Mn ceramics is optimal.

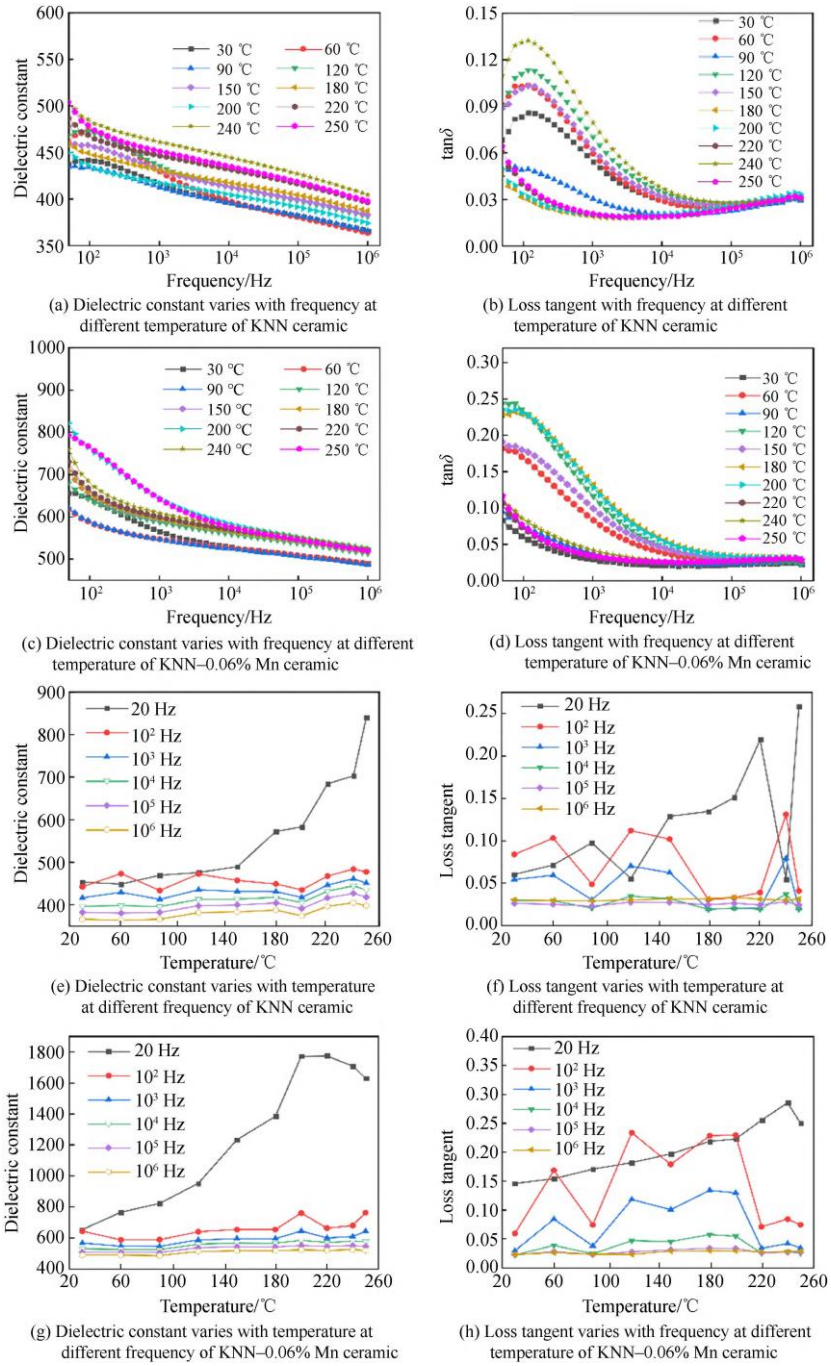

(a) Dielectric constant varies with frequency at different temperature of KNN ceramic

(b) Loss tangent with frequency at different temperature of KNN ceramic

(c) Dielectric constant varies with frequency at different temperature of KNN–0.06% Mn ceramic

(d) Loss tangent with frequency at different temperature of KNN–0.06% Mn ceramic

(e) Dielectric constant varies with temperature at different frequency of KNN ceramic

(f) Loss tangent varies with temperature at different frequency of KNN ceramic

(g) Dielectric constant varies with temperature at different frequency of KNN–0.06% Mn ceramic

(h) Loss tangent varies with frequency at different temperature of KNN–0.06% Mn ceramic

Figure 6 Dielectric permittivity and dielectric loss factor as functions of temperature of KNN ceramic and KNN ceramic doped with 0.060% MnO_2.

Figure 7 shows the conductivity variation curves of KNN-x%Mn ceramics with frequency at different temperatures. It is observable from Figure 7 that the conductivity of all ceramics gradually increases with frequency, primarily due to hopping conduction behavior [27]. Additionally, the conductivity of KNN-x%Mn ceramics does not increase significantly with temperature, further reflecting the high crystal stability of perovskite ceramics. Furthermore, MnO_2 doping indeed improves the conductivity of KNN ceramics to some extent, as MnO_2 doping causes lattice distortion, generating vacancies, interstitial ions, and other defects, thereby providing more channels and lower migration barriers for carrier transport.

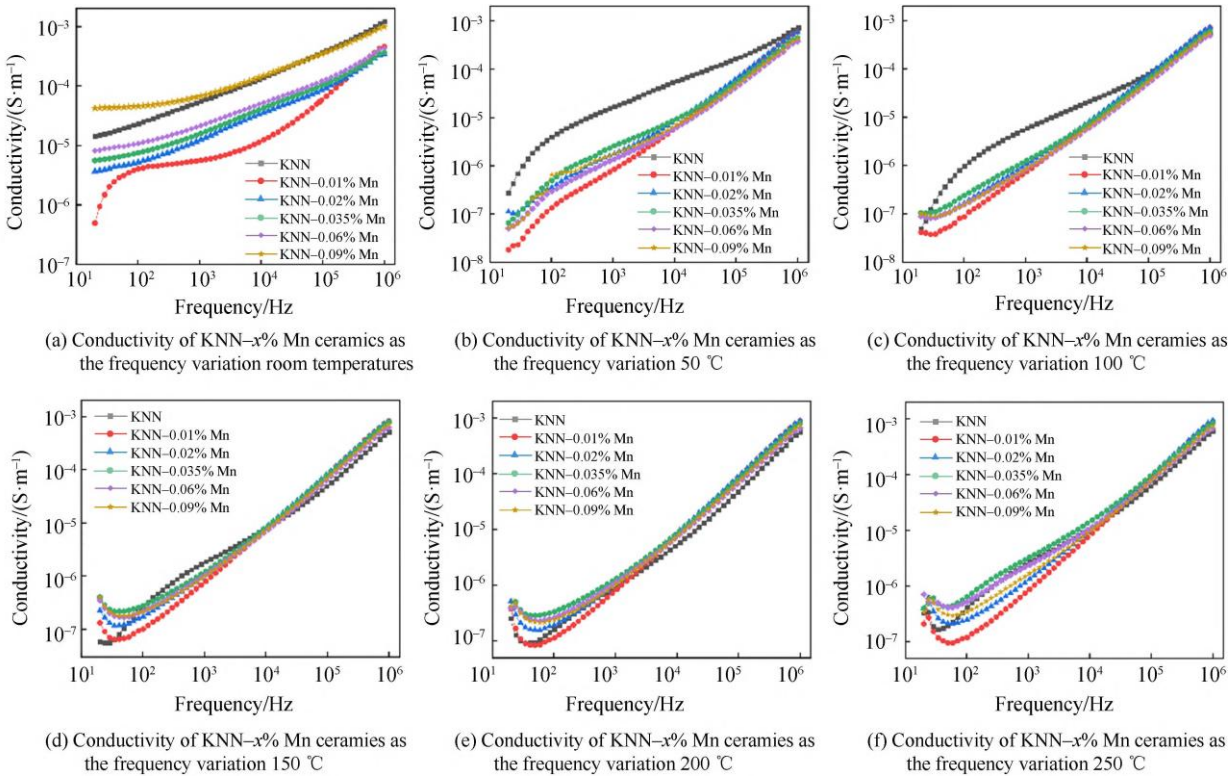

Figure 7 Conductivity of KNN-x%Mn ceramics as the frequency variation at different temperatures.

3.5 Non-Ohmic Characteristic Analysis

Figure 8 shows the non-Ohmic characteristics (nonlinear J−Echaracteristics) observed in KNN-x%Mn ceramic samples, defined by the relation given in reference [28]:

$$J=KE\alpha \quad (1)$$

Where: Eis the applied electric field; Jis the current density flowing through the sample; Kis a constant; αis the nonlinear coefficient. Results are summarized in Table 1. Compared with the nonlinear coefficient of 0.29 for pure KNN ceramics, the nonlinear coefficient of MnO_2-doped samples increases only slightly, primarily because the ordered sub-displacement of ion arrangement and electron polarization exhibit significant nonlinear effects. Furthermore, the high migration barrier and limited mobility of ferroelectric domain walls in KNN ceramics weaken their contribution to nonlinear conduction. More interestingly, prior to the occurrence of leakage current density, all ceramic samples experience a process of first decreasing and then increasing, as circled in Figure 8a. It is inferred that the conduction mechanism in this region may have shifted: under medium electric fields, it is dominated by electrical breakdown mechanisms (e.g., field emission); as the electric field further strengthens, thermal breakdown mechanisms begin to dominate. Joule heating effects cause continuous accumulation of heat generated by dielectric loss, leading to a continuous rise in local sample temperature, causing resistivity to drop and current to increase; the increased current further exacerbates heating, forming a positive feedback loop, eventually triggering thermal runaway of insulation performance and eventual electrical breakdown.

Table 1 Fitted parameters of nonlinear coefficient of the KNN-x%Mn ceramics

x(MnO_2)/%	0	0.010	0.020	0.035	0.060	0.095
α	0.298	0.421	0.362	0.421	0.342	0.421

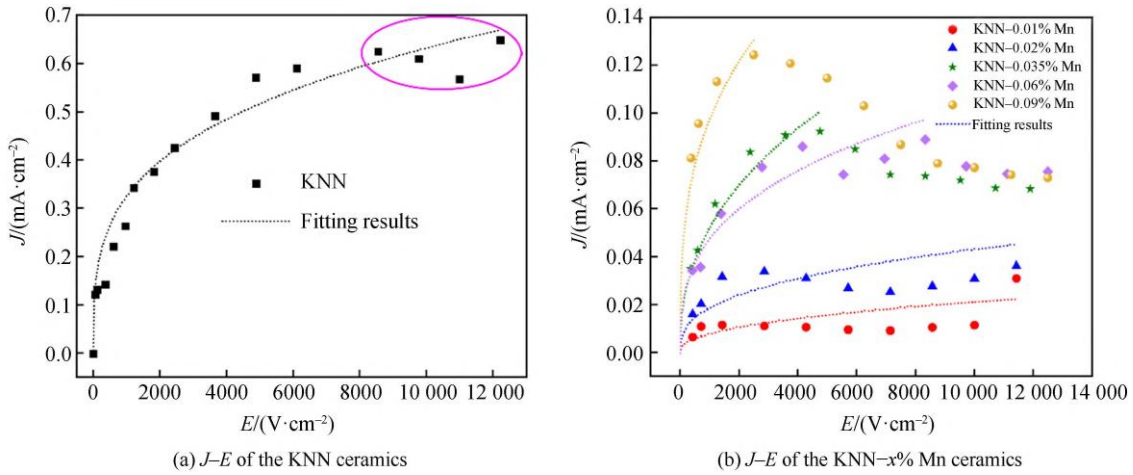

(a) *J–E* of the KNN ceramics (b) *J–E* of the KNN–*x*% Mn ceramics

Figure 8 Nonlinear J−Ebehaviors of the KNN-x%Mn ceramics.

3.6 Impedance Spectrum Characteristics Analysis

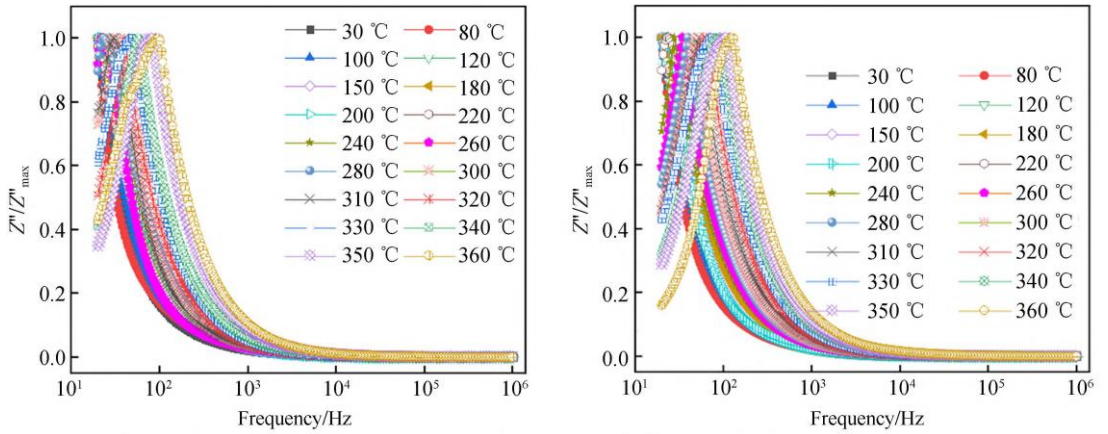

(a) *Z*''/*Z*''max for KNN crystals at various temperatures (b) *Z*''/*Z*''max for KNN–0.060% crystals at various temperatures

Figure 9 Frequency dependence of normalized imaginary parts (Z''/Zmax'') of impedance for KNN and KNN-0.060% Mn crystals at various temperatures.

Figure 9 shows the frequency dependence of the normalized imaginary part (Z''/Zmax'') of impedance for KNN and KNN-0.060%Mn crystals at different temperatures. It can be observed that both samples exhibit similar relaxation behavior at different temperatures. The Z''/Zmax'' spectra at each temperature point display an approximately symmetrical relaxation peak, and the characteristic frequency fmax corresponding to the relaxation peak shifts toward higher frequencies as temperature increases. This clearly indicates that the relaxation process is a thermally activated process. As temperature rises, the kinetic energy for dipole rotation or carrier (e.g., oxygen vacancies) migration increases, their relaxation time shortens, allowing them to keep pace with electric field changes and complete relaxation at higher external field frequencies. By plotting the Arrhenius relationship between the reciprocal of the characteristic frequency fmax, i.e., relaxation time τ, and 1000/T, the activation energy of this relaxation process can be calculated. Preliminary judgment suggests this relaxation process is closely related to oxygen vacancy migration or defect dipole reversal. The calculation results of

activation energy will provide key evidence for clarifying its specific atomic origin. The relaxation peak of the KNN-0.060%Mn sample is broadened and slightly asymmetric, implying a broad distribution of relaxation times, often associated with composition fluctuations or superposition of multiple relaxation processes caused by coexisting defects in the material.

This study establishes a concentration-dependent mechanistic framework demonstrating that MnO_2 doping optimizes the dielectric properties of $K_{0.5}Na_{0.5}NbO_3$ (KNN) ceramics by balancing microstructural densification, defect chemistry modulation, and domain dynamics, with 0.060 mol% emerging as the critical threshold for performance maximization. At the microstructural level, MnO_2 acts as a sintering aid at low concentrations (≤0.060%), forming low-melting eutectics with alkali oxides (e.g., Na_2O, K_2O) that trigger liquid-phase sintering. This shifts the sintering mechanism from slow solid-state diffusion to efficient dissolution-precipitation, promoting grain growth (average size: 1.2 μm → 3.5 μm) and reducing porosity, as confirmed by SEM. The increased densification minimizes pore-induced dielectric loss and enhances polarization efficiency, explaining the significant rise in dielectric constant (ε_r) at low frequencies (<10^2 Hz) for samples with ≤0.060% MnO_2. EDS mapping further reveals that Mn predominantly occupies B-sites (Nb^{5+} substitution) as Mn^{2+}/Mn^{3+}, with trace segregation at grain boundaries, while XRD confirms the retention of the tetragonal perovskite structure without impurity phases. This structural stability is foundational to the dielectric performance, as the tetragonal phase provides the necessary spontaneous polarization for ferroelectric response. However, exceeding 0.060% MnO_2 induces lattice distortion due to the mismatch in ionic radii between Mn ions (0.67 Å for Mn^{2+}, 0.58 Å for Mn^{3+}) and Nb^{5+} (0.69 Å), leading to increased defect density and reduced relative density. These microstructural changes correlate directly with the decline in ε_r and the rise in dielectric loss at 0.095% doping, highlighting the non-monotonic relationship between MnO_2 content and microstructural quality.

The dielectric response of MnO_2-doped KNN is governed by a complex interplay of polarization mechanisms, frequency dispersion, and temperature-dependent relaxation, which are modulated by Mn-induced defect dipoles and oxygen vacancies ($VO^{\bullet\bullet}$). At low frequencies (40 Hz–10^2 Hz), space charge polarization dominates, as charges accumulate at grain boundaries and defects, contributing to high ε_r. Here, 0.060% MnO_2 doping maximizes ε_r by reducing grain boundary resistance through densification and minimizing leakage current. As frequency increases (10^2–10^6 Hz), slower polarization mechanisms (e.g., space charge, dipole orientation) decouple from the alternating electric field, causing ε_r to decrease and stabilize—a behavior consistent with Debye relaxation theory. Dielectric loss (tan δ) follows an inverse relationship with frequency at low frequencies, attributed to reduced charge movement and leakage as electron mobility outpaces grain boundary polarization. The 0.060% sample exhibits the lowest tan δ across most frequencies, benefiting from homogeneous grain growth and minimized interfacial defects. However, at 0.095% MnO_2, tan δ rises sharply in the high-frequency range (10^2–10^6 Hz), likely due to grain boundary polarization, skin effect, and resonant frequency overlap, compounded by increased porosity and defect density. Temperature-dependent measurements reveal a universal trend: ε_r increases with temperature up to a threshold (240°C for pure KNN, 200°C for MnO_2-doped KNN) before declining, driven by enhanced dipole mobility at moderate temperatures and thermal disorder at higher temperatures. Notably, MnO_2 doping lowers the threshold temperature for optimal ε_r while stabilizing tan δ across 10^3–10^6 Hz, defining a practical operating window (200–240°C, 10^3–10^6 Hz) for electronic devices. Impedance spectroscopy further elucidates that relaxation peaks shift to higher frequencies with rising temperature, confirming a thermally activated process linked to $VO^{\bullet\bullet}$ migration or defect dipole reversal, with activation energy calculations supporting this mechanism.

The non-Ohmic and conductive behaviors of MnO_2-doped KNN provide additional insights into the role of Mn in modifying charge transport and breakdown resistance. All samples exhibit weakly nonlinear J-Echaracteristics (nonlinear coefficient α = 0.29–0.42), with MnO_2 doping slightly enhancing α compared to pure KNN (α = 0.29). This modest nonlinearity arises from the limited mobility of ferroelectric domain walls and the ordered sub-displacement of ions under high electric fields, which constrain contributions to nonlinear conduction. Conductivity measurements show a gradual increase with frequency across all temperatures, consistent with hopping conduction, where $VO^{\bullet\bullet}$ act as charge carriers. MnO_2 doping enhances conductivity by introducing lattice distortions and defects that lower migration barriers for carriers, though this effect is tempered by the countervailing reduction in porosity at optimal doping levels. A critical observation is the pre-breakdown current density trend: all samples first exhibit decreasing current before increasing under rising electric fields, indicating a shift from field emission (medium fields) to thermal breakdown (high fields). Joule heating from dielectric loss

accumulates locally, reducing resistivity and triggering a positive feedback loop of thermal runaway—a key failure mechanism for high-field applications. These findings have direct implications for device design: while MnO_2 doping improves low-frequency dielectric performance, excessive doping (≥0.095%) risks increased high-frequency loss and reduced breakdown strength, limiting its use in high-voltage MLCCs. Conversely, the 0.060% sample balances high ε_r, low tan δ, and stable temperature-frequency response, making it suitable for sensors, actuators, and filters operating in moderate-temperature environments. Future work should explore co-doping strategies (e.g., MnO_2 with Li^+ or Ta^{5+}) to further enhance temperature stability and high-frequency performance, while validating these lab-scale results in prototype devices. Overall, this study clarifies the multi-scale mechanisms by which MnO_2 modulates KNN ceramics, providing a roadmap for tailoring lead-free dielectrics to meet specific application requirements.

4. Conclusions

Focusing on lead-free piezoelectric material $K_{0.5}Na_{0.5}NbO_3$ (KNN) ceramics, this study investigated the regulatory effects of manganese dioxide (MnO_2) doping at different concentrations, acting as either a sintering aid or an acceptor dopant, on their structure and dielectric properties, highlighting the intrinsic connection of "material-structure-performance." The conclusions are as follows:

All doped samples retain the tetragonal perovskite structure. Appropriate doping significantly increases grain size, originating from liquid-phase sintering effects and lattice expansion caused by $Mn^{2+}/Mn^{3+}/Mn^{4+}$ substitution for Nb^{5+}.

Regarding dielectric properties, 0.060% is the optimal doping level. Samples doped at 0.060% concentration show significantly improved dielectric constants in the low-frequency region ($<10^2$ Hz), and grain homogenization and reduced leakage current lead to a substantial decrease in dielectric loss. However, in the high-frequency region (10^2–10^6 Hz), the 0.095% concentration doped sample exhibits slightly higher loss, attributed to grain boundary polarization and skin effects.

Temperature characteristics reveal: Dielectric constant decreases after increasing with temperature up to a threshold (240 °C for pure KNN; 200 °C for KNN-x%Mn), and dielectric loss changes stably within the 10–10^6 Hz frequency band, indicating that the 200–240 °C temperature range combined with high-frequency bands constitutes the optimal operating condition. Excessive doping leads to lattice deformation and new phase generation, causing density decline and performance degradation. Furthermore, MnO_2 doping can slightly enhance conductivity and the nonlinear coefficient.

In summary, MnO_2 doping, by optimizing microstructure and defect states, can significantly enhance the dielectric properties of KNN ceramics under clearly defined temperature or frequency windows, providing a material basis for the development of lead-free electronic devices.

References

[1] ZHU Dongze, LIU Yixuan, HUANG Haofeng, et al. Pressure-assisted sintering perovskite piezoelectric ceramics[J]. Journal of the Chinese Ceramic Society, 2025, 53(2): 451–470.
[2] WU Jiagang, WANG Ke, LI Fei. Advanced ferroelectric piezoelectric ceramics[J]. Journal of the Chinese Ceramic Society, 2022, 50(3): 555.
[3] YAO Fangzhou, WU Chaofeng, LI Jingfeng, et al. Application-oriented research progress of (K, Na)NbO_3-based lead-free piezoelectric ceramics[J]. Journal of the Chinese Ceramic Society, 2022, 50(3): 587–597.
[4] LI Haitao, LI Ran, WANG Guangxin, et al. Microwave preparation and properties of Ca-B co-doped KNN-based lead-free piezoelectric ceramics[J]. Journal of the Chinese Ceramic Society, 2020, 48(9): 1396–1404.
[5] WANG Mengli, SANG Xiujie, ZHOU Jing, et al. Effect of calcination temperature on piezoelectric properties of KNN-based ferroelectric ceramics[J]. Journal of the Chinese Ceramic Society, 2024, 52(6): 1935–1941.
[6] ZHAO R J, LI Y L, ZHENG Z S, et al. Phase structure regulation and enhanced piezoelectric properties of Li-doped KNN-based ceramics[J]. Materials Chemistry and Physics, 2020, 245: 122806.
[7] LEAL-PEREZ J E, HERRERA-PEREZ G, UMOH G V, et al. Band gap, complex dielectric function, and optical

properties of Sb-doped lead-free KNN piezo-ceramics analyzed by VEELS-TEM[J]. Materials Chemistry and Physics, 2022, 284: 126033.

[8] FUENTES J, PORTELLES J, DURRUTHY-RODRGUEZ M D, et al. Dielectric and piezoelectric properties of the KNN ceramic compound doped with Li, La and Ta[J]. Applied Physics A, 2015, 118(2): 709–715.

[9] XU F, CHEN J, LU Y M, et al. Exploration on the origin of enhanced piezoelectric properties in transition-metal ion doped KNN based lead-free ceramics[J]. Ceramics International, 2018, 44(14): 16745–16750.

[10] MGBEMERE H E, HERBER R P, SCHNEIDER G A. Effect of MnO_2 on the dielectric and piezoelectric properties of alkaline niobate based lead free piezoelectric ceramics[J]. Journal of the European Ceramic Society, 2009, 29(9): 1729–1733.

[11] ZHANG Zhaowei, JIANG Minhong, LI Lin, et al. Seedless solid-state growth, structure and electrical properties of Ta, Mn co-doped KNN-based piezoelectric single crystals[J]. Journal of the Chinese Ceramic Society, 2022, 50(9): 2358–2365.

[12] LI Dedong, JIANG Minhong, LI Lin, et al. Effect of cooling rate on structure and properties of KNN-based single crystals grown by seedless solid-state method[J]. Journal of the Chinese Ceramic Society, 2020, 48(9): 1446–1454.

[13] KIM J S, AHN C W, LEE S Y, et al. Effects of $LiNbO_3$ substitution on lead-free $(K_{0.5}Na_{0.5})NbO_3$ ceramics: Enhanced ferroelectric and electrical properties[J]. Current Applied Physics, 2011, 11(3): S149–S153.

[14] ZHAO Z H, DAI Y J, LI X L, et al. The evolution mechanism of defect dipoles and high strain in MnO_2-doped KNN lead-free ceramics[J]. Applied Physics Letters, 2016, 108(17): 172906.

[15] JIANG X P, CHEN Y, LAM K H, et al. Effects of MnO doping on properties of $0.97K_{0.5}Na_{0.5}NbO_3$–$0.03(Bi_{0.5}K_{0.5})TiO_3$ piezoelectric ceramics[J]. Journal of Alloys and Compounds, 2010, 506(1): 323–326.

[16] ORAYECH B, FAIK A, LOPEZ G A, et al. Mode-crystallography analysis of the crystal structures and the low- and high-temperature phase transitions in $Na_{0.5}K_{0.5}NbO_3$[J]. Journal of Applied Crystallography, 2015, 48(2): 318–333.

[17] SONG H C, CHO K H, PARK H Y, et al. Microstructure and piezoelectric properties of $(1–x)(Na_{0.5}K_{0.5})NbO_3$–$xLiNbO_3$ ceramics[J]. Journal of the American Ceramic Society, 2007, 90(6): 1812–1816.

[18] PARK H Y, AHN C W, CHO K H, et al. Low-temperature sintering and piezoelectric properties of CuO-added $0.95(Na_{0.5}K_{0.5})NbO_3$–$0.05BaTiO_3$ ceramics[J]. Journal of the American Ceramic Society, 2007, 90(12): 4066–4069.

[19] SUN X Y, DENG J X, CHEN J, et al. Effects of Li substitution on the structure and ferroelectricity of (Na, K)NbO_3[J]. Journal of the American Ceramic Society, 2009, 92(12): 3033–3036.

[20] DENG B Y, JIANG J H, LI H, et al. Enhanced piezoelectric property in Mn-doped $K_{0.5}Na_{0.5}NbO_3$ ceramics via cold sintering process and $KMnO_4$ solution[J]. Journal of the American Ceramic Society, 2022, 105(9): 5774–5782.

[21] MONIKA ANIZ I, MAISNAM M. Microwave sintering of MnO_2 added potassium sodium niobate ceramics and studies of their electrical properties[J]. Ferroelectrics, 2022, 588(1): 78–87.

[22] LOPEZ-JUAREZ R, GOMEZ-VIDALES V, CRUZ M P, et al. Dielectric, ferroelectric, and piezoelectric properties of Mn-doped $K_{0.5}Na_{0.5}NbO_3$ lead-free ceramics[J]. Journal of Electronic Materials, 2015, 44(8): 2862–2868.

[23] BIREY H. Dielectric properties of aluminum oxide films[J]. Journal of Applied Physics, 1978, 49(5): 2898–2904.

[24] KUMAR S, SHANDILYA M, THAKUR S, et al. Effect of Sol-gel synthesis method on the structural, electrical, and ferroelectric properties of lead-free $K_{0.5}Na_{0.5}NbO_3$ ceramic[J]. Journal of Sol-Gel Science and Technology, 2019, 92(1): 215–223.

[25] LI J Q, WANG J J, WU F M, et al. Microstructure and electric properties of Bi_2O_3-doped $(K_{0.5}Na_{0.5})NbO_3$ lead-free ceramics[J]. Coatings, 2022, 12(4): 526.

[26] SHARMA J P, KUMAR D, SHARMA A K. Structural and dielectric properties of pure potassium sodium niobate (KNN) lead free ceramics[J]. Solid State Communications, 2021, 334: 114345.

[27] CHINNATHAMBI M, SAKTHISABARIMOORTHI A, JOSE M, et al. Study of the electrical and dielectric behaviour of selenium doped CCTO ceramics prepared by a facile sol-gel route[J]. Materials Chemistry and Physics, 2021, 272: 124970.

[28] SWATSITANG E, PUTJUSO S, PUTJUSO T. Effect of Mg^{2+} and Sr^{2+} doping on dielectric and non-ohmic properties in binary compound $CaCu_3Ti_4O_{12}/TiO_2$ ceramics[J]. Results in Physics, 2024, 64: 107955.